Hindawi
International Journal of Chemical Engineering
Volume 2022, Article ID 3139696, 13 pages
https://doi.org/10.1155/2022/3139696

Research Article

Dry Reforming of Methane with Mesoporous Ni/ZrO_2 Catalyst

Subhan Azeem,[1] **Rabya Aslam**,[2] **and Mahmood Saleem**[2]

[1]*Chemical Engineering Department, NFC IET Multan, Multan, Pakistan*
[2]*Institute of Chemical Engineering & Technology, University of the Punjab, Lahore 54590, Pakistan*

Correspondence should be addressed to Subhan Azeem; msazeem@nfciet.edu.pk

Received 30 September 2022; Revised 29 November 2022; Accepted 2 December 2022; Published 16 December 2022

Academic Editor: Ho Soon Min

Dry reforming of methane has exhibited significant environmental benefits as it utilizes two major greenhouse gases (CO_2 and CH_4) to produce synthesis gas, a major building block for hydrocarbons. This process has gained industrial attention as catalyst deactivation due to coke deposition being a major hindrance. The present study focuses on the dry reforming of methane over Ni-supported mesoporous zirconia support. Ni metal was loaded over in-house synthesized mesoporous zirconia within the 0–15 wt % range using the wet impregnation method. The physicochemical properties of the synthesized catalysts were studied using various characterization techniques, namely, XRD, SEM, FTIR, TGA, and N_2 adsorption-desorption techniques. The activity of all the catalysts was evaluated at 750°C and gas hourly space velocity (GHSV) of 72000 ml/h/g_{cat} for 9 hours (540 min). The deactivation factor indicating a loss in conversion with time is reported for each catalyst. 10 wt% Ni/ZrO_2 showed the highest feed conversion of about 68.8% for methane and 70.2% for carbon dioxide and the highest stability (15.1% deactivation factor and 21% weight loss) for dry reforming of methane to synthesis gas.

1. Introduction

Almost 85% of the total world's energy comes from fossil fuels. Nevertheless, the combustion of fossil fuels has caused numerous problems, denoted as global warming [1–3]. CH_4 and CO_2 are two major greenhouse gases that contribute to global warming [4, 5]. Dry reforming of methane (DRM) is a catalytic conversion method, utilizing these gases and converting them to syngas (CO and H_2 gas) [6, 7]. The main reaction is displayed in (1), whereas the side reactions are given in equations (2)–(4) [8]. Equation (2) represents the disproportionation reaction, while equation (3) denotes the methane cracking reaction. Equation (4), commonly termed as reverse water-gas shift reaction, is the key method for the H_2O formation [9]. DRM is an endothermic reaction that entails the use of high temperatures, which favors rapid catalyst deactivation and thus lowers its industrial applications. This aspect renders the CH_4 to decompose and the coke to form as shown in the following equations:

$$CH_4 + CO_2 \leftrightarrow 2CO + 2H_2 \Delta H^0 = 248\,\text{kJ mol}^{-1}, \quad (1)$$

$$2CO \longrightarrow C + CO_2 \Delta H^0 = -172\,\text{kJ mol}^{-1}, \quad (2)$$

$$CH_4 \longrightarrow C + 2H_2 \Delta H^0 = 75\,\text{kJ mol}^{-1}, \quad (3)$$

$$CO_2 + H_2 \longrightarrow CO + H_2O \Delta H^0 = -41\,\text{kJ mol}^{-1}. \quad (4)$$

Investigators made enormous efforts to synthesize suitable catalysts for DRM to decrease the formation of coke. Noble metals-based catalysts showed excellent coke resistance and higher conversions for DRM. However, due to their limited availability and higher cost, the use of noble metals-based catalysts is limited. Researchers alternatively used non-noble metals-based catalysts like nickel-based catalysts for the reforming process [10–14]. Many investigators synthesized catalysts by using numerous supports such as Al_2O_3 and ZrO_2 [15]. Another property of catalyst support that is found to be very useful for reforming

methane is oxygen storage capacity because supports that provide O_2 could improve the coke oxidation over a metal surface. Thus, oxygen vacancies improved the CO_2 conversion into CO on the catalyst surface [16–18]. The catalyst stability is dictated via the correspondence between the extent of carbon removal and the degree of CH_4 breakdown [19]. Hence, zirconia generally presents significant ionic conductivity due to its higher thermal stability and provides oxygen vacancies. ZrO_2 is among the most universally used zirconium compounds in nature. Its phases of crystallization comprise cubic, monoclinic, and tetragonal at ambient pressure [20–22]. Thus, using stable support like zirconia promotes oxygen vacancy and stability of Ni-formed catalysts [23]. Therdthianwong et al. studied the effect of ZrO_2 as catalyst support for DRM [24]. The study revealed that ZrO_2 considerably enhanced the catalyst stability in the view of superior coke resistance by improving the dissociation of O_2 intermediates which then react with carbon species formed over the metal. Abasaeed et al. studied the effect of catalyst calcination temperature supported on zirconia and ceria in DRM [25]. Catalysts calcined at low temperatures showed high activity and yield, while catalysts at high temperatures showed lower activity and yield. Wolfbeisser et al. investigated DRM over zirconia–ceria-supported nickel catalyst [26]. Results revealed that Ni/ZrO_2 catalyst showed enhanced activity, stability, and lower coke formation. Ibrahim et al. conducted a study to investigate the DRM process over Ni-based catalysts supported by zirconia [27]. The results indicated that the zirconia support source has a greater influence on the overall performance of the DRM process. Pompeo et al. studied the stability enhancement of Ni-based catalysts supported on ZrO_2 and or CeO_2 for the reforming process. They found that the addition of support decreases the deactivation by sintering, conferring to the system with a higher contribution of adsorbed oxygen species, favoring the deposited carbon elimination [28]. Though, it has been a less focused area and has not been studied systematically despite its promising results in producing syngas.

2. Materials and Methods

2.1. Catalyst Preparation. To synthesize mesoporous zirconia, zirconium (IV) n-butoxide ((80 wt.% solution in 1-butanol) was used as the precursor. Approximately 5.0 g of (EO)20(PO)70(EO)20 triblock copolymer (Pluronic P123 from BASF, Co.) was dissolved in 50.0 mL of 99.5+% anhydrous ethanol (Acros Organics) and allowed to stir for 4 h at room temperature until dissolved completely. Then, approximately 80 ml of zirconium (IV) n-butoxide ((80 wt.% solution in 1-butanol) was dissolved in 20 mL of 68–70 wt % nitric acid and 50.0 mL of anhydrous ethanol. The solution was stirred at room temperature for 4 hours. Solvent evaporation was performed at 100°C for 24 h in the oven without stirring. Finally, the catalyst was calcined under air in the furnace at 500°C temperature for 5 h.

Zirconia support was then used to load nickel within the range of 0–15 wt % using the wet impregnation method [29]. For this purpose, nickel (II) nitrate hexahydrate Ni $(NO_3)_2.6H_2O$ was used as a metal precursor. The calculated amount of Ni-salt was dissolved in water, and then, the calculated amount of zirconia support was added to the solution. The resulting mixture is stirred continuously for 3 hours at room temperature (26°C ± 2°C). After completing 3 hours, the mixture is placed in an oven for drying for about 24 hours at 5°C. To keep the relative homogeneousness of the mixture, the slurry is stirred manually after every hour until most of the water is removed during the initial 6 hours of drying as lack of stirring in this initial stage often results in agglomeration of the catalyst [30]. The final dried catalyst is crushed, sieved, and calcined in dry air at 800°C for 5 hours, at a heating rate of 5°C·min^{-1}. Finally, the calcined catalysts obtained are named C-0, C-2, C-4, C-6, C-8, C-10, C-12, and C-15 with the number representing the amount of Ni wt % loaded over in-house synthesized zirconia. The flowchart for the preparation of the catalyst through the impregnation method is shown in Figure 1.

2.2. Characterization of the Catalyst. N_2 adsorption/desorption isotherm determines the texture properties like specific surface area, pore size, and pore volume of all synthesized catalysts at (−196°C) of liquid nitrogen via the Brunauer–Emmett–Teller (BET) based surface analyzer (Nova 2200e Quanta chrome). The material was first degassed in a vacuum at 300°C for 3 h before analysis. The crystal structure of all synthesized Ni/ZrO_2 catalysts was determined with high accuracy through X-ray diffraction (XRD) with the help of an advanced diffractometer (Bruker D2-Phaser). This diffractometer has a 10–80° (2θ) detection range and operates between 200 mA and 40 kV by using Cu Kα radiation. Fourier transform infrared spectroscopy of the synthesized catalyst was recorded in the range of 400–4000 cm^{-1} on the Shimadzu 8400 FTIR spectrometer with KBr pellets at room temperature. Scanning electron microscope images were obtained via FEI titan 200, USA & NOVA NANOSEM 430, respectively, to determine particle morphology. Thermal analysis was carried out at the end of the reaction to estimate the quantity of carbon that was deposited on the used catalyst samples. The analysis was performed with a thermogravimetric/differential analyzer (Shimadzu TGA). For TGA analysis, 10 mg of the samples were heated from room temperature up to 1000°C at a heating rate of 25°C/minute, and the weight change was recorded with temperature rise.

2.3. Experimental Setup. The activity of synthesized catalysts for the dry reforming of methane was carried out in a fixed-bed reactor as shown in Figure 2. Before the reaction, the catalyst was in situ reduced with hydrogen gas at 550°C for two hours at a flow rate of 50 ml/min. The reaction was carried out at atmospheric pressure, and the reactant gas composition was 50 mol % methane (99.995%) and 50 mol % CO_2 (99.995%). Gas hourly space velocity and other reaction conditions (T = 750°C and

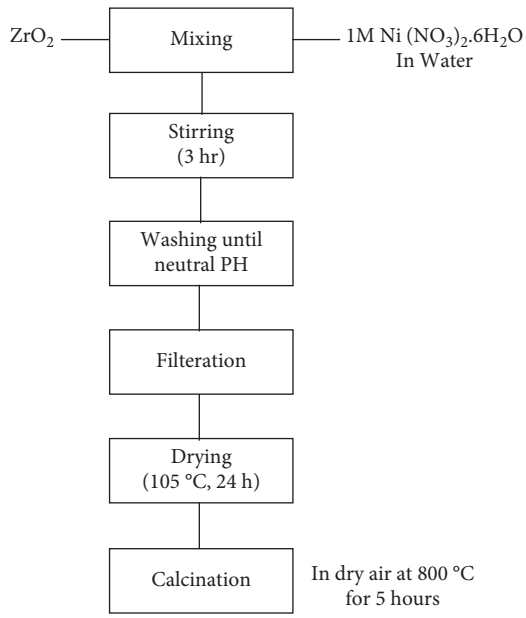

Figure 1: Wet impregnation method flowchart.

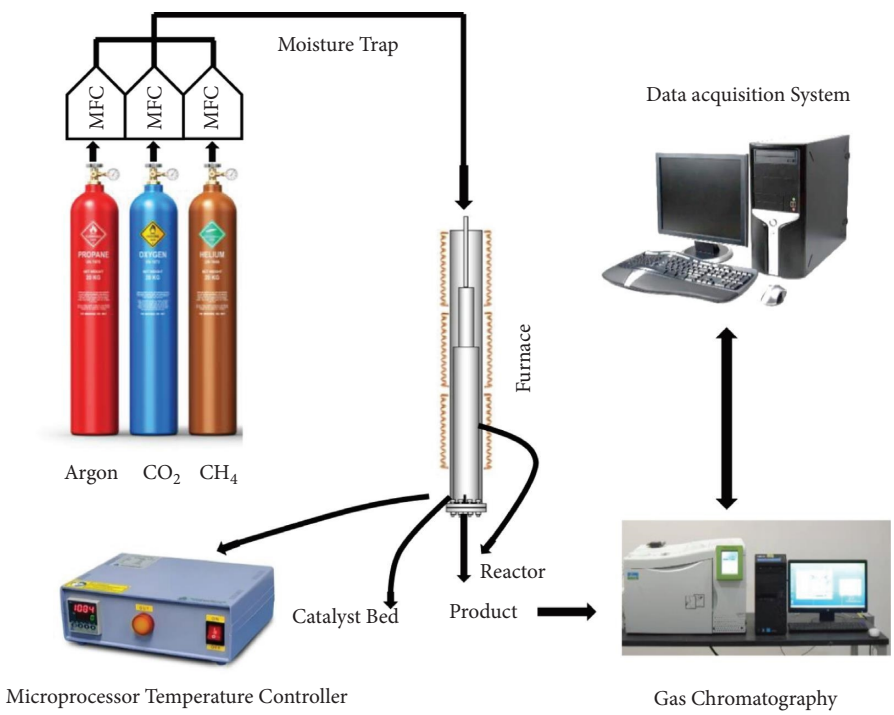

Figure 2: Schematic diagram of the reactant and products analysis.

$P = 1$ bar) were kept constant for each catalyst. The temperature was determined with a thermocouple inserted inside the reactor. The reactor was fitted with a gas chromatograph which was equipped with a thermal conductivity detector (GC-TCD) to analyze the composition of exhaust gases coming out from the reactor. Helium was used as a carrier gas in a gas chromatograph. Methane, carbon dioxide conversions, and H_2/CO ratio were determined via the following formulas:

$$X_{CH_4}(\%) = 100 \times \frac{F_{CH_4 in} - F_{CH_4 out}}{F_{CH_4 in}}, \quad (5)$$

$$X_{CO_2}(\%) = 100 \times \frac{F_{CO_2 in} - F_{CO_2} out}{F_{CO_2 in}}, \quad (6)$$

$$\frac{H_2}{CO} = \frac{F_{H_2} out}{F_{CO} out}. \quad (7)$$

Table 1: Textural properties of the catalyst.

Catalyst	S_g (m^2/g)	BJH v_p (cm^3/g)	BJH d_p (nm)
C-0	54.0	0.16	21.2
C-2	43.8	0.14	20.8
C-4	36.0	0.13	19.8
C-6	34.9	0.13	19.7
C-8	34.5	0.12	18.9
C-10	32.9	0.11	16.9
C-12	20.2	0.07	9.0
C-15	11.2	0.05	6.8

S_g is the surface area by using the BET method, BJH v_p is the BJH adsorption cumulative volume of the pore between 17 Å and 3000 Å width, and BJH d_p is the BJH adsorption average pore diameter.

Also, the deactivation factor (DA, %) for the catalyst at a particular temperature was calculated using the following equation:

$$\mathrm{DA} = 100 \times \frac{Xi_{CH_4} - Xf_{CH_4}}{Xi_{CH_4}}, \quad (8)$$

where X_{i,CH_4} represents the initial conversion at temperature T and X_{f,CH_4} represents the final conversion at temperature T.

3. Results

3.1. Characterization of Fresh Catalysts

3.1.1. BET. Pore size distribution and surface area of synthesized catalysts were obtained through the nitrogen adsorption-desorption study. Surface area and pore volume are presented in Table 1. The surface area of mesoporous zirconia was found to be 54 m^2/g which is comparable to literature-reported values [31, 32], and it was observed that there is a decrease in the surface area and the pore volume when active metal was added to it. This indicates that Ni particles fill up the pores of support to reduce their surface area and pore volume.

The average pore size distribution of all the catalysts falls between mesopores, mesopores >2 nm, and mespores <50 nm range. The mesopores structure in metal catalysts played a vital role to restrict the formation of metallic crystallite and also the sintering of metallic particle surface at a higher temperature during the reaction [33]. The N_2 adsorption-desorption isotherms are presented in Figure 3. All the catalysts are representing type IV isotherm with characteristic H_2 hysteresis. In the area of lower relative pressure, the isotherms of catalysts show a linear increase in adsorbed amount with an increase in relative pressure. This shows the monolayer adsorption of N_2 on the pore walls [6]. However, a steep increase in the area of higher relative pressure from 0.73–0.99 in the adsorption branch of the isotherms can be observed in the figure. It represents the filling up of the mesopores by the adsorbed nitrogen. Pore size distribution is presented in Figure 4. All the catalysts show the formation of the mesostructured in the presence of a surface-active agent used in the synthesis of pristine zirconia.

3.1.2. X-Ray Diffraction (XRD). XRD studies were made to determine the crystal phase in the catalyst structure. The XRD patterns of all fresh catalysts are shown in Figures 5(a) and 5(b). Both monoclinic and tetragonal zirconia phases are identified on the support and the other samples. Peaks appear at 2θ angles that are equivalent to 28.2, 31.5, 34.2, 34.3, and 40.6° ascribed as the monoclinic phase (111) of ZrO_2 [JCPDS 88-2390]. Similarly, tetragonal phases are observed at 29.9, 34.9, 42.88, 50.09, and 59.5° ascribed as the tetragonal phase (111), (220) of ZrO_2 [JCPDS 14-0534]. Similar peaks were also observed in different studies conducted for Ni-ZrO_2 catalyst prepared by the impregnation method [34–36]. It was observed that with impregnation of even a small amount of Ni (2 wt %), the intensity of the peaks for monoclinic zirconia was a bit reduced, and also, it was transformed to a tetragonal phase. The reduction in intensity was enhanced with an increase in Ni loading on zirconia support. The peaks at $2\theta = 37.3°$, 42.8°, 62.9°, and 75.3° are due to the presence of NiO species [JCPDS 22-1189].

3.1.3. Fourier Transform Infrared Spectroscopy. FTIR spectroscopy is very helpful to evaluate the presence of functional groups in the sample. Figure 6(a) depicts the FTIR spectra for pristine zirconia support, while Figure 6(b) shows the FTIR spectra of fresh catalysts, respectively. A wide spectrum of 3431 cm^{-1} is due to the –OH bend indicating water absorption on the sample surface. A peak around 2968 cm^{-1} shows the presence of C–H bonding in the sample. The peak at 1624 cm^{-1} and 1363 cm^{-1} confirm the presence of –OH stretching and bending modes, indicating the presence of a hydroxyl group present on the zirconia surface. The peak at 879 cm^{-1} and further a wide band around 800–500 cm^{-1} corresponds to zirconia. Peaks at 1503 cm^{-1} show O-H stretching which is the characteristic of Ni $(OH)_2$ [37].

3.1.4. Scanning Electron Microscopy. The surface morphology of each of the catalysts is given by the SEM images shown in Figure 7. It can be observed from images that support exhibiting of the cubic structure which is preserved in all samples with metal loading. With the increased metal loading, clusters of particles are observable (Figures 7(d)–7(g)). Metal particles seems to be uniformly distributed over zirconia support [38, 39].

3.2. Catalyst Performance. The catalyst activity in terms of CH_4 and CO_2 conversion in the presence of pristine zirconia and synthesized catalyst with nickel loading was studied at a temperature of 750°C. Initially, thermodynamic conversion

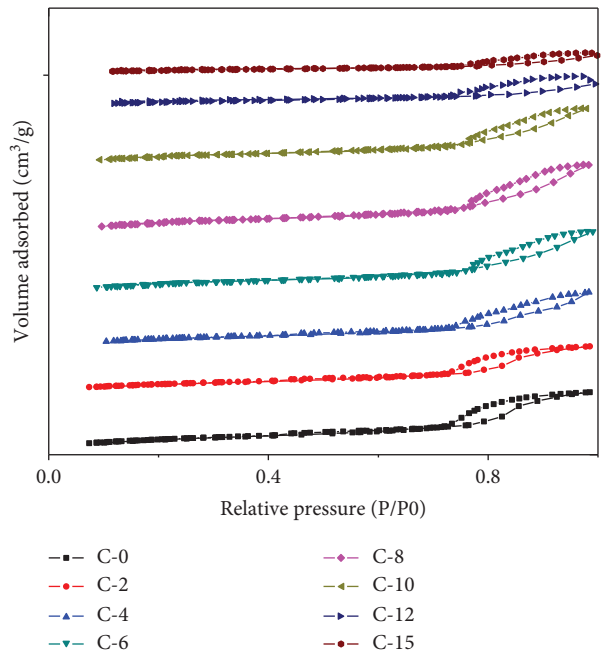

Figure 3: N_2 adsorption-desorption isotherm of catalysts.

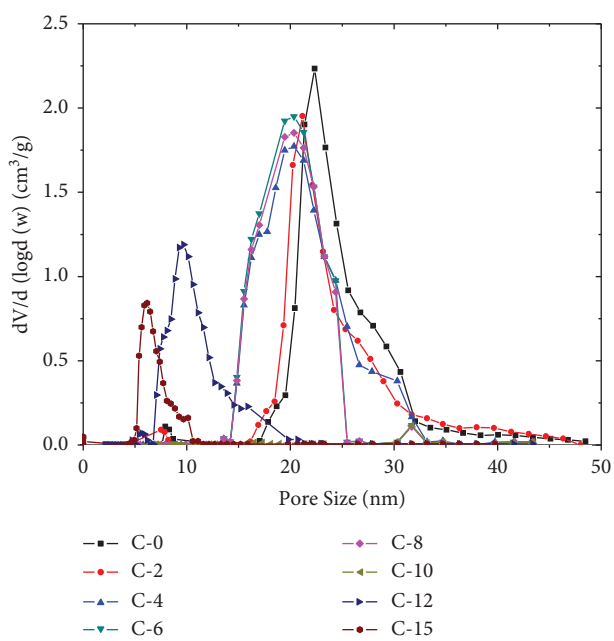

Figure 4: Pore size distribution plots.

with a no-coke deposition assumption was calculated, showing the maximum achievable conversion for DRM reaction for methane and carbon dioxide for any catalyst (Figure 8(a)).

The activity of pristine mesoporous zirconia (C-0) was evaluated within a temperature range of 600 to 800°C and conversion for both methane and carbon dioxide is reported after 10 minutes in Figure 8(b). It was observed that conversion is very little affected after rising in temperature from 750°C to 800°C; therefore, rest of the catalyst activity experiments were performed at 750°C. Also, from equilibrium conversion, the difference in conversion after 750°C is not much (at 750°C, its 94% for CO_2 and at 800°C, its 95.1% for CO_2).

The activity results in terms of CH_4 and CO_2 conversion for all catalysts are shown in Figures 8(c) and 8(d), as a function of time at a temperature of 750°C. The reaction was carried out for 9 hours (540 min). 10% Ni/ZrO_2 catalyst shows the highest methane and carbon dioxide conversion at a reaction temperature of 750°C at any time in comparison to other catalysts.

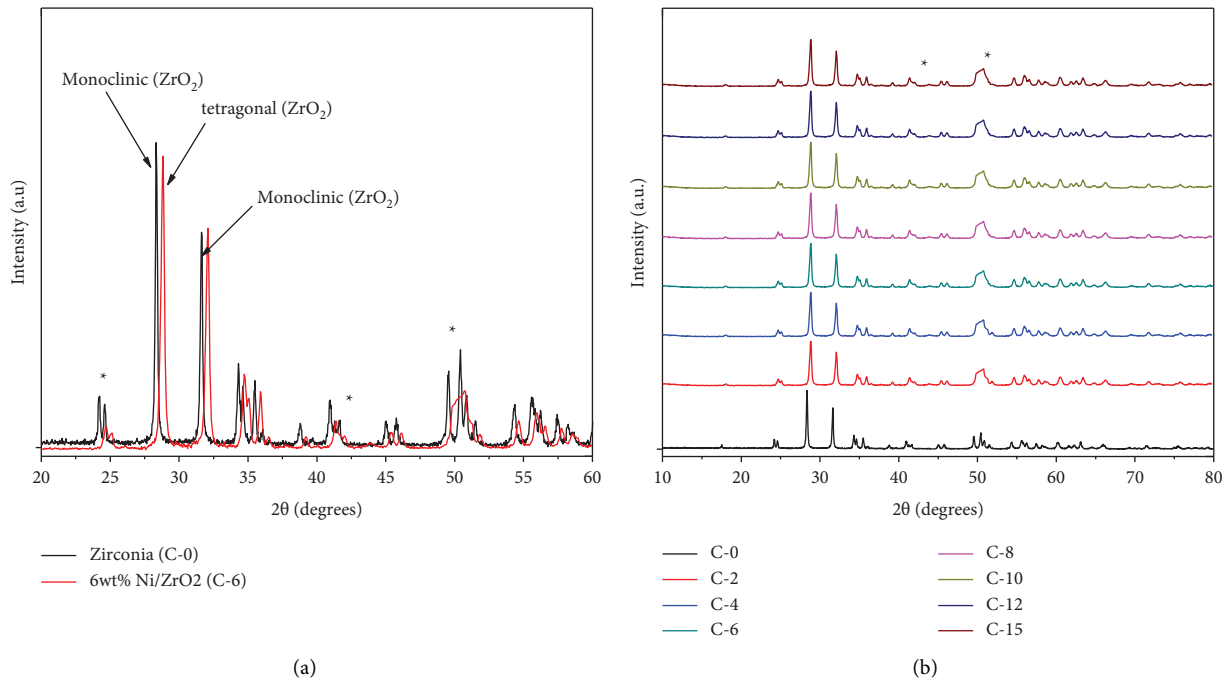

Figure 5: (a) XRD patterns of synthesized calcined Ni-loaded zirconia (6 wt % Ni/ZrO_2) with pristine zirconia (*peaks changed due to the presence of Ni). (b) XRD patterns of synthesized freshly calcined catalysts.

Pan et al. reported 69% conversion for methane with 10%Ni/Al_2O_3, but the deactivation factor was very high even after 2 hours of experiment [40]. The previous studies reported that at lower GHSV, the conversion will be higher due to more contact time and vice versa. For instance, Jin et al. reported 36% conversion at low GHSV of 6000 ml/h·g_{cat} over MgO-promoted Ni/Al_2O_3 and 800°C. Ibrahim et al. reported in 2021, the 54% conversion of methane for DRM reaction over various catalysts [27, 41, 42]. Fakeeha et al. reported 70% methane conversion over Ni/H-ZSM-5 at 86,000 ml/h·g_{cat} GHSV and 760°C [43]. The highest conversion of CH_4 obtained in this study is 68.8% which is comparable to the literature-reported conversions. The molar ratio of H_2/CO in the product stream is reported in Figure 8(e). Theoretically, it can be equal to one but because of the reverse water-gas shift reaction, the Boudouard reaction and methane gas decomposition reaction ratio can be less than 1 [44]. For pristine zirconia, the H_2/CO ratio was within the range of 0.67–0.72 during reaction time, and for catalysts with metal loading, the ratio was observed close to 1. For 10 wt % Ni over zirconia, the ratio varies from 0.96 to 0.98 during a reaction time of 9 hours.

It was observed that pristine zirconia's activity was the lowest in comparison to other catalysts. The deactivation factor was calculated for each catalyst with initial conversion at 10 minutes and final conversion at 540 minutes. The deactivation factor for pristine zirconia was the highest as 27% less conversion was observed just after two hours. With the increase in Ni metal loading over zirconia, conversion for both methane and carbon dioxide was increased and the maximum was observed with C-10. After 10 wt% loadings, although the deactivation factor was not affected much, high metal loading conversion starts decreasing. For instance, with 15 wt % Ni loading, conversion drops to 55% for methane. This might be attributed to the lower surface area due to particle agglomeration with high metal loading. Deactivation factor results are tabulated in Table 2.

As observed from activity experimental results, the deactivation of catalysts might be due to coke deposition on catalysts surface. The coke formation results in the accumulation of inactive species of carbon on the catalyst surface as observed from the deactivation factor. The presence of Ni prevents the formation of coke during the reforming process as the deactivation factor was low in the presence of Ni over zirconia. The deactivation 10 wt% Ni/ZrO_2 was 15.1% after 540 minutes in comparison to 36.4% with pristine zirconia. The increase in Ni-contents, reduction of pore volume, and surface area show that agglomeration of Ni particles reduces the active sites and results in lower conversions.

Although the deactivation factor was comparable after 10 wt % Ni loading, indicating Ni's impact on the stability of the catalyst (Table 2), conversion was dropped, which might be attributed to low surface area (Table 1). Zirconia itself shows higher stability as compared to other literature reported due to its amphoteric nature along with the presence of mobile oxygen species [45]. Comparison of the effect of temperature on the catalyst performance with the literature is shown in Table 3. It is apparent that this catalyst provides a higher product yield than those catalysts operated at given reaction conditions.

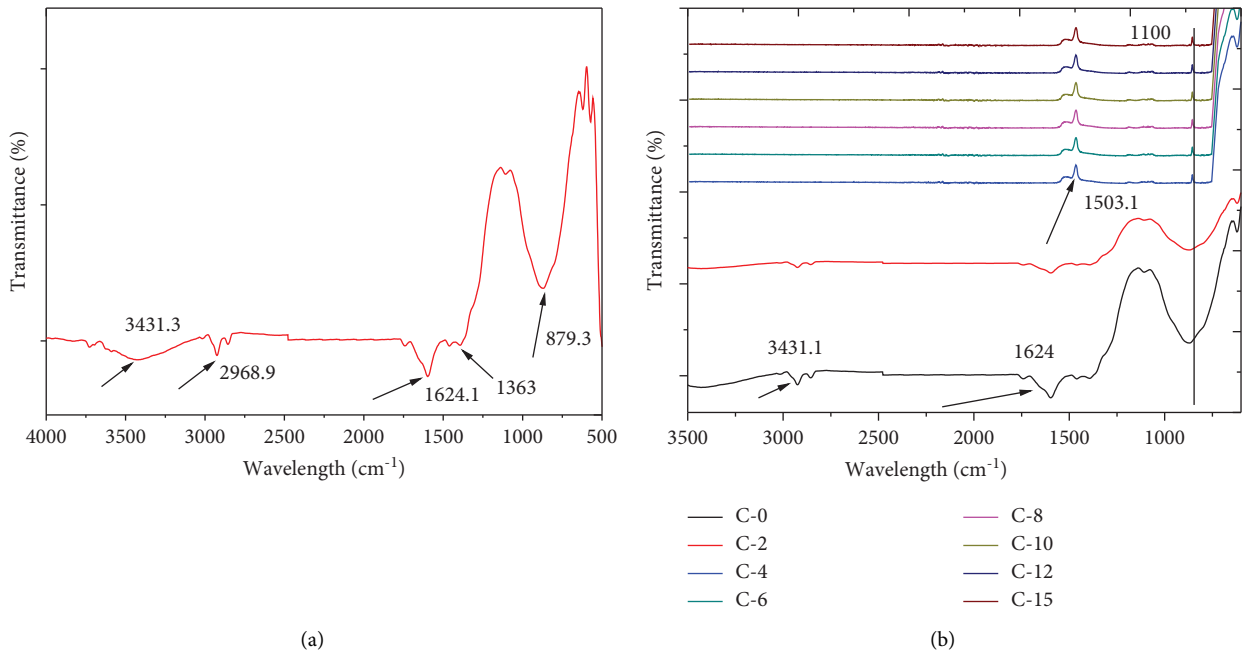

Figure 6: (a) FTIR spectra for pristine zirconia support. (b) FTIR spectra of synthesized freshly calcined catalysts.

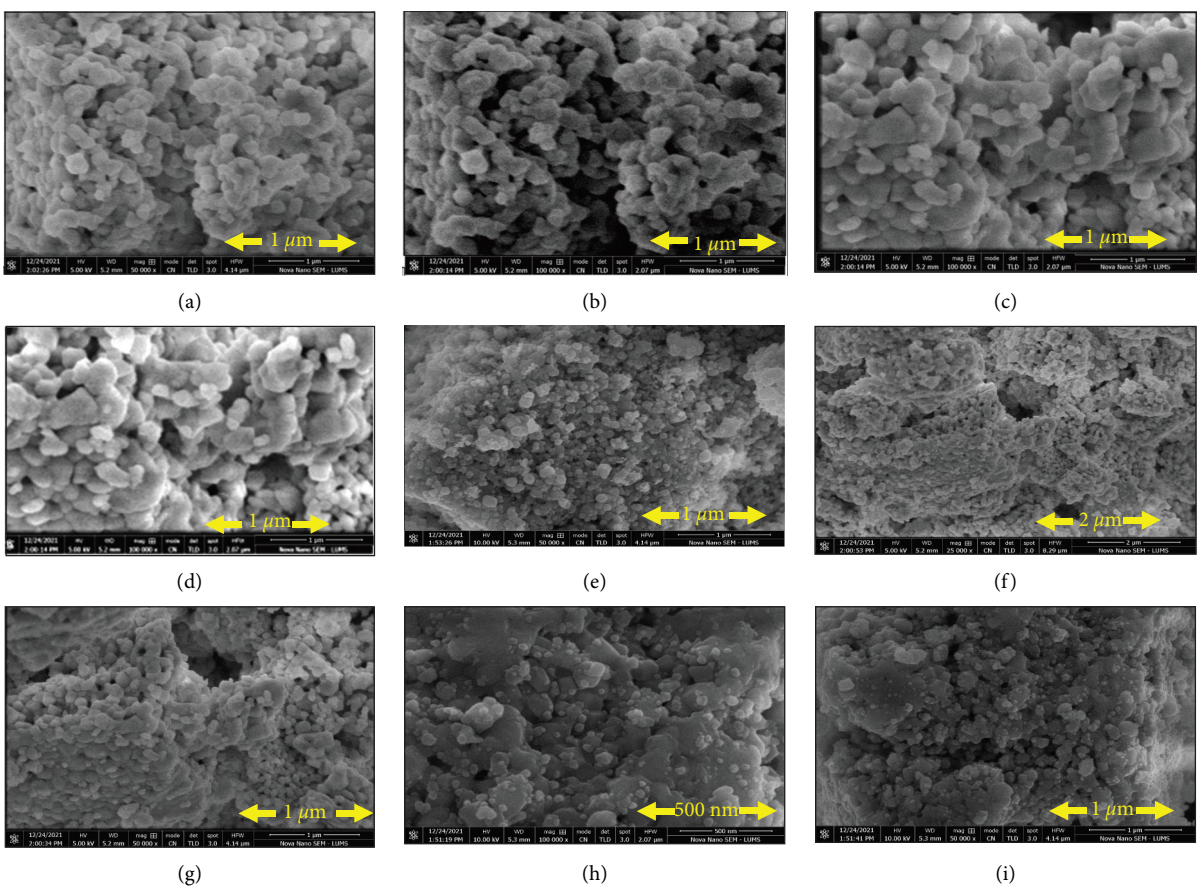

Figure 7: SEM images of fresh catalysts: (a) C-0, (b) C-2, (c) C-4, (d) C-6, (e) C-8, (f)–(h) C-10, and (i) C-15.

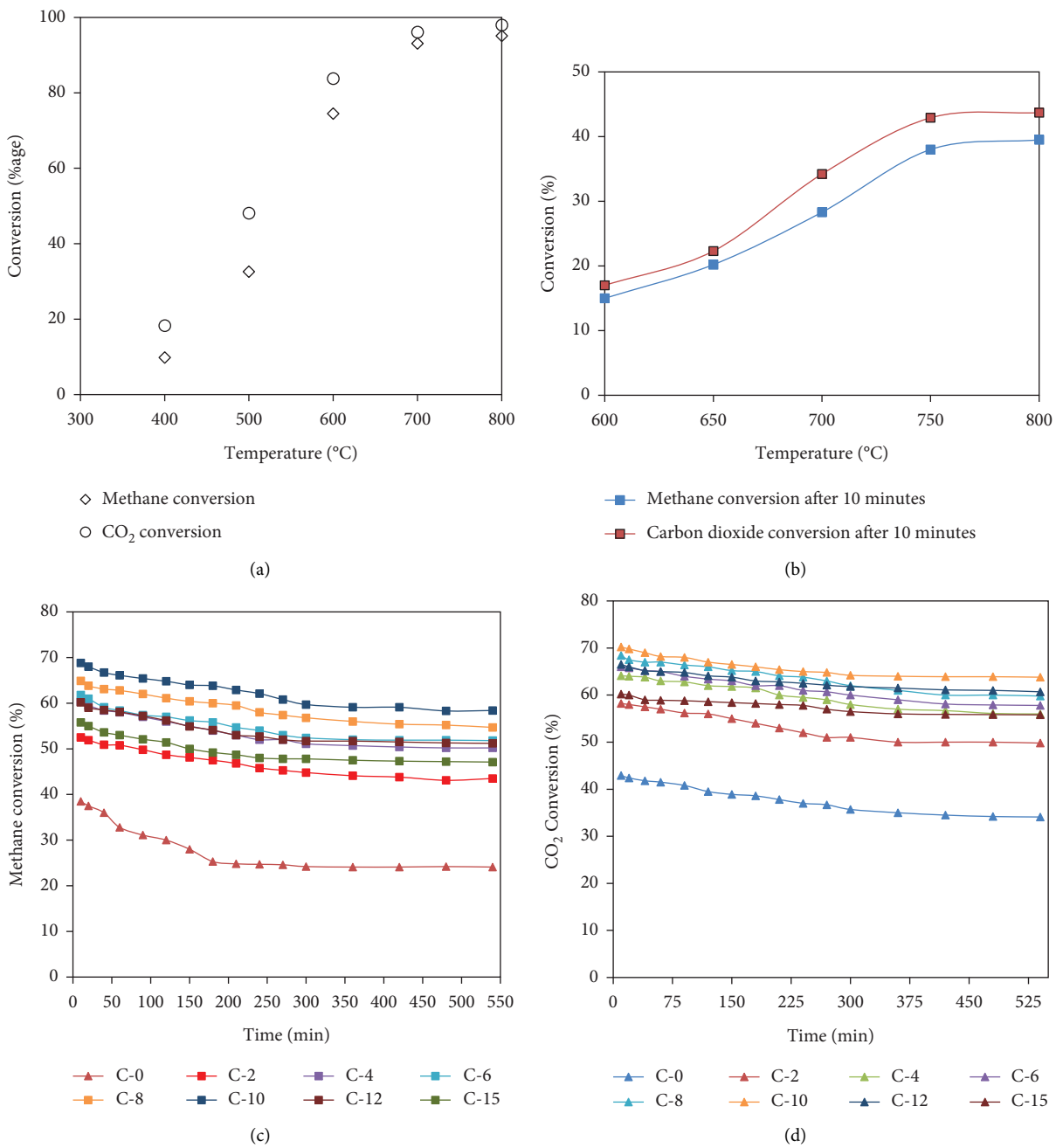

Figure 8: Continued.

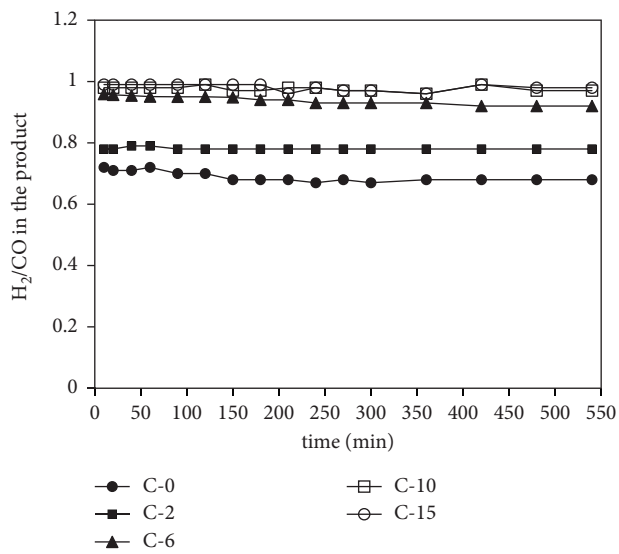

(e)

Figure 8: (a) Equilibrium conversion as a function of temperature. (b) Activity of pristine zirconia support within a temperature range of 600–800°C with GHSV 72000 ml/hr·g_{cat}. (c) Activity of synthesized catalysts in terms of %CH4 conversion as a function of time at a temperature ($T = 750$°C, $p = 1$ bar, GHSV = 72000 ml·h^{-1}·g_{cat}^{-1}). (d) Activity of synthesized catalysts in terms of %age CO_2 conversion as a function of time at a temperature ($T = 750$°C, $p = 1$ bar, GHSV = 72000 ml·h^{-1}·g_{cat}^{-1}). (e) H_2/CO ratio in the product stream ($T = 750$°C, $p = 1$ bar, GHSV = 72000 ml·h^{-1}·g_{cat}^{-1}).

Table 2: Conversion and deactivation factors for synthesized catalysts.

Catalysts	CH_4 conversion (X_{CH4})		CO_2 conversion (X_{CO2})		Deactivation factor (DA) (%)
	Initial (%)	Final (%)	Initial (%)	Final (%)	
C-0	38.5	24.1	42.9	34.1	36.4
C-2	52.5	43.5	58.2	49.8	17.1
C-4	62.3	52.2	64.1	56	16.2
C-8	64.9	54.5	68.4	59.8	16.0
C-10	68.8	58.4	70.2	63.8	15.1
C-12	60.2	51.2	66.5	60.9	15.0
C-15	55.8	47.1	60.2	55.8	15.6

3.3. Characterization of Spent Catalyst

3.3.1. Thermogravimetric Analysis. Thermal analysis was performed to determine the quantity of carbon deposited on the spent catalyst, and the results of weight loss curves are presented in Figure 9, conducted in the presence of air. The TGA profile indicates two regions of catalyst weight loss, one minor and the second major. The Ist region of minor/slight weight loss occurred at the 50–380°C temperature range due to the water absorbed and surface carbon and coke comprising hydrogen species due to oxidation [2, 34, 61–64].

Major weight loss began at approximately 500°C and ended within 740–800°C for spent catalysts containing active metals, and the combustion of carbon deposits continued until around 850°C for spent Pristine zirconia catalyst. The zirconia had the highest amount of carbon deposits of about 57.9%, while after 10 wt %, weight loss was approximately 21%. It was observed that with the increase in active metal, carbon deposition decreased. Zirconia itself deposited 58% carbon which is less in comparison to other supports such as silica where up to 80% carbon deposition is reported, and it might be attributed to the higher oxygen density of zirconia which could gasify carbon deposits [34, 35].

Table 3: Performance comparison with that of other studies.

Catalyst	Reaction temperature (°C)	CH_4 conversion (%)	Ref.
Ni-Al_2O_3	800	36	[41]
Ni-SiO_2	800	50	[42]
Ni-MgO	760	70	[43]
Ni-H-ZSM-5	700	76	[46]
15% Ni/perlite + Zr	700	79	[47]
0.1% Ni/Ce + Zr	850	38	[48]
5% Ni/La + Zr	700	66	[49]
15% Ni + Co/Al + -Zr^{-1}	850	72	[50]
5% Ni + Co/Al + Zr	550	18	[51]
5% Ni/PO_4+Zr	800	45	[12]
Ni/Al_2O_3	700	53	[52]
Ni/MCM-41	800	85	[53]
Ni/SiO_2	700	41	[40]
3 wt.% Ni/SBA-15	800	72	[54]
Ni/La + Zr	700	70	[49]
$La_{0.9}$ $Ce_{0.9}Ni_{0.9}Zr_{0.1}$ O_3	750	40	[55]
$La_{0.9}$ $Ce_{0.9}Ni_{0.7}Zr_{0.3}$ O_3	750	10	[55]
Ni-CeO_2	760	65	[56]
Ni-ZrO_2	750	64	[57]
Ni-ZrO_2	700	30	[58]
SiO_2@Ni-ZrO_2	700	43	[59]
Ni-ZrO_2	700	54	[27]
5% Ni/Y + Zr	700	63	[60]
Ni-ZrO_2	750	68.8	Present study

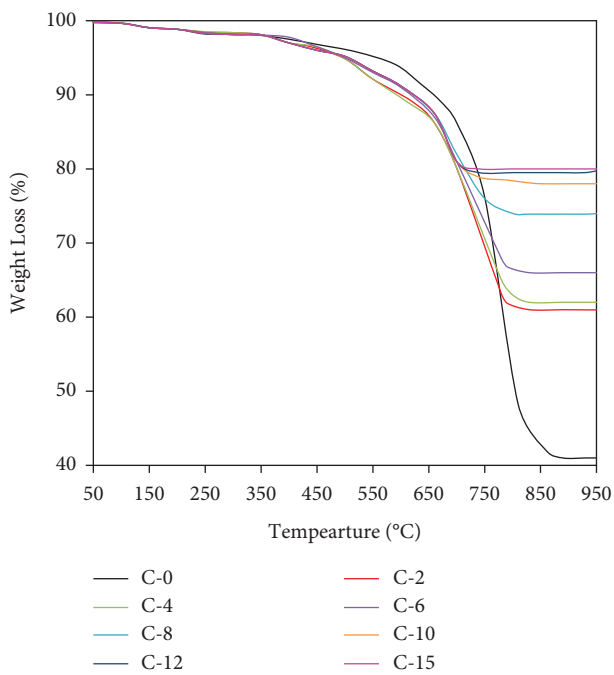

Figure 9: TGA profile of all spent catalysts.

4. Conclusion

In the present study, mesoporous zirconia was in-house synthesized and then loaded with active metal Ni within the range of 0–15 wt % to check its activity and selectivity for DRM reaction. 10% Ni/ZrO_2 catalyst shows higher performance among catalysts catalyst during DRM with the lowest deactivation factor after 540 minutes of reaction. Methane and carbon dioxide conversions were higher compared to the series of catalysts evaluated in the study within 9 hours of the experiment. The application of mesoporous ZrO_2 as support for low-cost Ni particles exhibited better performance and a superior role in dry reforming of methane reaction.

Data Availability

The experimental and characterization data used to support the findings of this study are included within the article.

Conflicts of Interest

The authors declare that they have no conflicts of interest.

References

[1] L. Teh, H. Setiabudi, S. Timmiati, M. Aziz, N. Annuar, and N. Ruslan, "Recent progress in ceria-based catalysts for the dry reforming of methane: a review," *Chemical Engineering Science*, vol. 242, Article ID 116606, 2021.

[2] M. García-Diéguez, I. Pieta, M. Herrera, M. Larrubia, and L. Alemany, "Nanostructured Pt-and Ni-based catalysts for CO_2-reforming of methane," *Journal of Catalysis*, vol. 270, no. 1, pp. 136–145, 2010.

[3] A. K. Karmaker, M. M. Rahman, M. A. Hossain, and M. R. Ahmed, "Exploration and corrective measures of greenhouse gas emission from fossil fuel power stations for Bangladesh," *Journal of Cleaner Production*, vol. 244, Article ID 118645, 2020.

[4] U. Shahzad, Z. Fareed, F. Shahzad, and K. Shahzad, "Investigating the nexus between economic complexity, energy consumption and ecological footprint for the United States: new insights from quantile methods," *Journal of Cleaner Production*, vol. 279, Article ID 123806, 2021.

[5] M. Springmann, D. Mason-D'Croz, S. Robinson et al., "Mitigation potential and global health impacts from emissions pricing of food commodities," *Nature Climate Change*, vol. 7, no. 1, pp. 69–74, 2017.

[6] J. Watson, Y. Zhang, B. Si, W. T. Chen, and R. de Souza, "Gasification of biowaste: a critical review and outlooks," *Renewable and Sustainable Energy Reviews*, vol. 83, pp. 1–17, 2018.

[7] V. S. Sikarwar, M. Zhao, P. S. Fennell, N. Shah, and E. J. Anthony, "Progress in biofuel production from gasification," *Progress in Energy and Combustion Science*, vol. 61, pp. 189–248, 2017.

[8] A. Al–Fatish, A. Ibrahim, A. Fakeeha, M. Soliman, M. Siddiqui, and A. Abasaeed, "Coke formation during CO_2 reforming of CH_4 over alumina-supported nickel catalysts," *Applied Catalysis A: General*, vol. 364, no. 1-2, pp. 150–155, 2009.

[9] A. Abasaeed, S. Kasim, W. Khan et al., "Hydrogen yield from CO_2 reforming of methane: impact of La_2O_3 doping on supported Ni catalysts," *Energies*, vol. 14, no. 9, p. 2412, 2021.

[10] R. Patel, A. S. Al-Fatesh, A. H. Fakeeha et al., "Impact of ceria over WO_3–ZrO_2 supported Ni catalyst towards hydrogen production through dry reforming of methane," *International Journal of Hydrogen Energy*, vol. 46, no. 49, pp. 25015–25028, 2021.

[11] A. S. Al-Fatesh, A. H. Fakeeha, A. A. Ibrahim, and A. E. Abasaeed, "Ni supported on La_2O_3+ ZrO_2 for dry reforming of methane: the impact of surface adsorbed oxygen species," *International Journal of Hydrogen Energy*, vol. 46, no. 5, pp. 3780–3788, 2021.

[12] A. A. Ibrahim, A. S. Al-Fatesh, W. U. Khan et al., "Enhanced coke suppression by using phosphate-zirconia supported nickel catalysts under dry methane reforming conditions," *International Journal of Hydrogen Energy*, vol. 44, no. 51, pp. 27784–27794, 2019.

[13] H. Ay and D. Üner, "Dry reforming of methane over CeO_2 supported Ni, Co and Ni–Co catalysts," *Applied Catalysis B: Environmental*, vol. 179, pp. 128–138, 2015.

[14] M. Usman, W. Wan Daud, and H. F. Abbas, "Dry reforming of methane: influence of process parameters—a review," *Renewable and Sustainable Energy Reviews*, vol. 45, pp. 710–744, 2015.

[15] S. Das, S. Thakur, A. Bag, M. S. Gupta, P. Mondal, and A. Bordoloi, "Support interaction of Ni nanocluster based catalysts applied in CO_2 reforming," *Journal of Catalysis*, vol. 330, pp. 46–60, 2015.

[16] E. Faria, R. Neto, R. Colman, and F. Noronha, "Hydrogen production through CO_2 reforming of methane over Ni/$CeZrO_2$/Al_2O_3 catalysts," *Catalysis Today*, vol. 228, pp. 138–144, 2014.

[17] N. Abdel Karim Aramouni, J. Zeaiter, W. Kwapinski, J. Leahy, and M. N. Ahmad, "Molybdenum and nickel-molybdenum nitride catalysts supported on MgO-Al_2O_3 for the dry reforming of methane," *Journal of CO_2 Utilization*, vol. 44, Article ID 101411, 2021.

[18] C. Papadopoulou, H. Matralis, and X. Verykios, "Utilization of biogas as a renewable carbon source: dry reforming of methane," *Catalysis for alternative energy generation*, pp. 57–127, Springer, New York NY, USA, 2012.

[19] S. M. Stagg-Williams, F. B. Noronha, G. Fendley, and D. E. Resasco, "CO_2 reforming of CH_4 over Pt/ZrO_2 catalysts promoted with La and Ce oxides," *Journal of Catalysis*, vol. 194, no. 2, pp. 240–249, 2000.

[20] J. D. McCullough and K. N. Trueblood, "The crystal structure of baddeleyite (monoclinic ZrO_2)," *Acta Crystallographica*, vol. 12, no. 7, pp. 507–511, 1959.

[21] D. K. Smith and C. F. Cline, "Verification of existence of cubic zirconia at high temperature," *Journal of the American Ceramic Society*, vol. 45, no. 5, pp. 249-250, 1962.

[22] A. Chen, Y. Zhou, S. Miao, Y. Li, and W. Shen, "Assembly of monoclinic ZrO_2 nanorods: formation mechanism and crystal phase control," *CrystEngComm*, vol. 18, no. 4, pp. 580–587, 2016.

[23] T. A. Maia, J. M. Assaf, and E. M. Assaf, "Performance of cobalt catalysts supported on $CexZr_{1-x}O_2$ ($0< x< 1$) solid solutions in oxidative ethanol reforming," *Reaction Kinetics, Mechanisms and Catalysis*, vol. 109, no. 1, pp. 181–197, 2013.

[24] S. Therdthianwong, A. Therdthianwong, C. Siangchin, and S. Yongprapat, "Synthesis gas production from dry reforming of methane over Ni/Al_2O_3 stabilized by ZrO_2," *International Journal of Hydrogen Energy*, vol. 33, no. 3, pp. 991–999, 2008.

[25] A. E. Abasaeed, A. S. Al-Fatesh, M. A. Naeem, A. A. Ibrahim, and A. H. Fakeeha, "Catalytic performance of CeO_2 and ZrO_2 supported Co catalysts for hydrogen production via dry reforming of methane," *International Journal of Hydrogen Energy*, vol. 40, no. 21, pp. 6818–6826, 2015.

[26] A. Wolfbeisser, O. Sophiphun, J. Bernardi, J. Wittayakun, K. Fottinger, and G. Rupprechter, "Methane dry reforming over ceria-zirconia supported Ni catalysts," *Catalysis Today*, vol. 277, pp. 234–245, 2016.

[27] A. A. Ibrahim, A. Fakeeha, A. Abasaeed, and A. Al-Fatesh, "Dry reforming of methane using Ni catalyst supported on ZrO_2: the effect of different sources of zirconia," *Catalysts*, vol. 11, no. 7, p. 827, 2021.

[28] F. Pompeo, D. Gazzoli, and N. N. Nichio, "Stability improvements of Ni/α-Al_2O_3 catalysts to obtain hydrogen from methane reforming," *International Journal of Hydrogen Energy*, vol. 34, no. 5, pp. 2260–2268, 2009.

[29] K. Selvarajah, N. H. H. Phuc, B. Abdullah, F. Alenazey, and D. V. N. Vo, "Syngas production from methane dry reforming over Ni/Al_2O_3 catalyst," *Research on Chemical Intermediates*, vol. 42, no. 1, pp. 269–288, 2016.

[30] Y. Huang and J. Schwarz, "The effect of catalyst preparation on catalytic activity: II. The design of Ni/Al_2O_3 catalysts prepared by wet impregnation," *Applied Catalysis*, vol. 30, no. 2, pp. 255–263, 1987.

[31] M. L. Chaudhary, A. S. Al-Fatesh, R. Kumar et al., "Promotional effect of addition of ceria over yttria-zirconia supported Ni based catalyst system for hydrogen production through dry reforming of methane," *International Journal of Hydrogen Energy*, vol. 47, no. 48, pp. 20838–20850, 2022.

[32] A. S. Al-Fatesh, R. Patel, V. K. Srivastava et al., "Barium-Promoted Yttria–Zirconia-Supported Ni Catalyst for Hydrogen Production via the Dry Reforming of Methane: Role of Barium in the Phase Stabilization of Cubic ZrO2," *American chemical society omega*, vol. 7, no. 9, pp. 16468–16483, 2022.

[33] W. J. Jang, J. O. Shim, H. M. Kim, S. Y. Yoo, and H. S. Roh, "A review on dry reforming of methane in aspect of catalytic properties," *Catalysis Today*, vol. 324, pp. 15–26, 2019.

[34] R. K. Singha, A. Shukla, A. Yadav et al., "Energy efficient methane tri-reforming for synthesis gas production over highly coke resistant nanocrystalline $Ni–ZrO_2$ catalyst," *Applied Energy*, vol. 178, pp. 110–125, 2016.

[35] C. G. Anchieta, E. M. Assaf, and J. M. Assaf, "Effect of ionic liquid in Ni/ZrO_2 catalysts applied to syngas production by methane tri-reforming," *International Journal of Hydrogen Energy*, vol. 44, no. 18, pp. 9316–9327, 2019.

[36] M. Zhang, J. Zhang, Y. Wu et al., "Insight into the effects of the oxygen species over Ni/ZrO_2 catalyst surface on methane reforming with carbon dioxide," *Applied Catalysis B: Environmental*, vol. 244, pp. 427–437, 2019.

[37] J. Coates, *Interpretation of Infrared Spectra, a Practical Approach*, Coates Consulting, Newtown, USA, 2000.

[38] D. M. Walker, S. L. Pettit, J. T. Wolan, and J. N. Kuhn, "Synthesis gas production to desired hydrogen to carbon monoxide ratios by tri-reforming of methane using Ni–MgO–(Ce, Zr)O_2 catalysts," *Applied Catalysis A: General*, vol. 445-446, pp. 61–68, 2012.

[39] M. A. Goula, N. Charisiou, G. Siakavelas et al., "Syngas production via the biogas dry reforming reaction over Ni supported on zirconia modified with CeO_2 or La_2O_3 catalysts," *International Journal of Hydrogen Energy*, vol. 42, no. 19, pp. 13724–13740, 2017.

[40] C. Pan, Z. Guo, H. Dai, R. Ren, and W. Chu, "Anti-sintering mesoporous Ni–Pd bimetallic catalysts for hydrogen production via dry reforming of methane," *International Journal of Hydrogen Energy*, vol. 45, no. 32, pp. 16133–16143, 2020.

[41] B. Jin, S. Li, and X. Liang, "Enhanced activity and stability of MgO-promoted Ni/Al_2O_3 catalyst for dry reforming of methane: role of MgO," *Fuel*, vol. 284, Article ID 119082, 2021.

[42] Y. Xu, X.J. Du, P. Wang et al., "A comparison of Al_2O_3 and SiO_2 supported Ni-based catalysts in their performance for the dry reforming of methane," *Journal of Fuel Chemistry and Technology*, vol. 47, no. 2, pp. 199–208, 2019.

[43] A. H. Fakeeha, W. U. Khan, A. S. Al-Fatesh, and A. E. Abasaeed, "Stabilities of zeolite-supported Ni catalysts for dry reforming of methane," *Chinese Journal of Catalysis*, vol. 34, no. 4, pp. 764–768, 2013.

[44] M. Radlik, M. Adamowska-Teyssier, A. Krzton et al., "Dry reforming of methane over $Ni/Ce_{0.62}Zr_{0.38}O_2$ catalysts: effect of Ni loading on the catalytic activity and on H_2/CO production," *Comptes Rendus Chimie*, vol. 18, no. 11, pp. 1242–1249, 2015.

[45] N. A. K. Aramouni, J. G. Touma, B. A. Tarboush, J. Zeaiter, and M. N. Ahmad, "Catalyst design for dry reforming of methane: analysis review," *Renewable and Sustainable Energy Reviews*, vol. 82, pp. 2570–2585, 2018.

[46] T. Zhang, Z. Liu, Y. A. Zhu et al., "Dry reforming of methane on Ni-Fe-MgO catalysts: influence of Fe on carbon-resistant property and kinetics," *Applied Catalysis B: Environmental*, vol. 264, Article ID 118497, 2020.

[47] F. Mesrar, M. Kacimi, L. F. Liotta, F. Puleo, and M. Ziyad, "Syngas production from dry reforming of methane over ni/perlite catalysts: effect of zirconia and ceria impregnation," *International Journal of Hydrogen Energy*, vol. 43, no. 36, pp. 17142–17155, 2018.

[48] J. Sun, D. Yamaguchi, L. Tang et al., "Enhancement of oxygen exchanging capability by loading a small amount of ruthenium over ceria-zirconia on dry reforming of methane," *Advanced Powder Technology*, vol. 33, no. 2, Article ID 103407, 2022.

[49] A. S. Al-Fatesh, Y. Arafat, A. A. Ibrahim et al., "Catalytic behaviour of Ce-doped Ni systems supported on stabilized zirconia under dry reforming conditions," *Catalysts*, vol. 9, no. 5, p. 473, 2019.

[50] C. Le Quéré, R. M. Andrew, P. Friedlingstein et al., "Global carbon budget 2018," *Earth System Science Data*, vol. 10, no. 4, pp. 2141–2194, 2018.

[51] W. Y. Kim, Y. H. Lee, H. Park, Y. H. Choi, M. H. Lee, and J. S. Lee, "Coke tolerance of Ni/Al_2O_3 nanosheet catalyst for dry reforming of methane," *Catalysis Science and Technology*, vol. 6, no. 7, pp. 2060–2064, 2016.

[52] F. S. Al-Mubaddel, R. Kumar, M. L. Sofiu et al., "Optimizing acido-basic profile of support in Ni supported La_2O_3+ Al_2O_3 catalyst for dry reforming of methane," *International Journal of Hydrogen Energy*, vol. 46, no. 27, pp. 14225–14235, 2021.

[53] A. S. Al-Fatesh, R. Kumar, S. O. Kasim et al., "Effect of cerium promoters on an MCM-41-supported nickel catalyst in dry reforming of methane," *Industrial & Engineering Chemistry Research*, vol. 61, no. 1, pp. 164–174, 2021.

[54] H. Setiabudi, K. H. Lim, N. Ainirazali, S. Y. Chin, and N. H. N. Kamarudin, "CO_2 reforming of CH_4 over Ni/SBA-15: influence of Ni loading on the metal-support interaction and catalytic activity," *Journal of Materials and Environmental Science*, vol. 8, no. 2, pp. 573–581, 2017.

[55] P. Dezvareh, H. Aghabozorg, M. Hossaini Sadr, and K. Zare, "Synthesis, characterization, and catalytic performance of $La_{1-x}C_{ex}Ni_{1-y}ZryO_3$ perovskite nanocatalysts in dry reforming of methane," *Oriental Journal of Chemistry*, vol. 34, no. 3, pp. 1469–1477, 2018.

[56] M. Yu, Y. A. Zhu, Y. Lu, G. Tong, K. Zhu, and X. Zhou, "The promoting role of Ag in Ni-CeO_2 catalyzed CH4-CO_2 dry reforming reaction," *Applied Catalysis B: Environmental*, vol. 165, pp. 43–56, 2015.

[57] X. Zhang, Q. Zhang, N. Tsubaki, Y. Tan, and Y. Han, "Carbon dioxide reforming of methane over Ni nanoparticles incorporated into mesoporous amorphous ZrO_2 matrix," *Fuel*, vol. 147, pp. 243–252, 2015.

[58] P. Kumar, Y. Sun, and R. O. Idem, "Nickel-based ceria, zirconia, and ceria–zirconia catalytic systems for low-temperature carbon dioxide reforming of methane," *Energy and Fuels*, vol. 21, no. 6, pp. 3113–3123, 2007.

[59] J. Dou, R. Zhang, X. Hao et al., "Sandwiched SiO2@ Ni@ ZrO_2 as a coke resistant nanocatalyst for dry reforming of

methane," *Applied Catalysis B: Environmental*, vol. 254, pp. 612–623, 2019.

[60] A. A. Ibrahim, A. H. Fakeeha, M. S. Lanre et al., "The effect of calcination temperature on various sources of ZrO_2 supported Ni catalyst for dry reforming of methane," *Catalysts*, vol. 12, no. 4, p. 361, 2022.

[61] R. Zanganeh, M. Rezaei, and A. Zamaniyan, "Dry reforming of methane to synthesis gas on NiO–MgO nanocrystalline solid solution catalysts," *International Journal of Hydrogen Energy*, vol. 38, no. 7, pp. 3012–3018, 2013.

[62] C. Bozo, N. Guilhaume, E. Garbowski, and M. Primet, "Combustion of methane on CeO_2–ZrO_2 based catalysts," *Catalysis Today*, vol. 59, no. 1-2, pp. 33–45, 2000.

[63] C. E. Hori, H. Permana, K. Y. Simon, A. Brenner, and D. Belton, "Thermal stability of oxygen storage properties in a mixed CeO_2-ZrO_2 system," *Applied Catalysis B: Environmental*, vol. 16, no. 2, pp. 105–117, 1998.

[64] A. Djaidja, S. Libs, A. Kiennemann, and A. Barama, "Characterization and activity in dry reforming of methane on NiMg/Al and Ni/MgO catalysts," *Catalysis Today*, vol. 113, no. 3-4, pp. 194–200, 2006.